Dynamic Soil-Structure Interaction Analysis under Seismic Loads Using the Scaled Boundary Finite-Element Method

Mohammad Hossein Bazyar[1*] and Bahareh Basirat[2]

1. Assistant Professor, Department of Civil Engineering, Yasouj University, Yasouj, Iran,
*Corresponding Author; email: mhbazyar@mail.yu.ac.ir
2. Post Graduate Student, Department of Civil Engineering, Yasouj University, Yasouj, Iran

Received: 14/11/2011
Accepted: 19/06/2012

ABSTRACT

The novel scaled boundary finite-element method is a fundamental solution-less boundary-element method based on finite element technology, which combines the advantages of finite-element and boundary element methods. Only the boundary is discretized reducing the special discritization by one as in the boundary element method; no fundamental solution is required as in the finite-element method; and the radiation condition at the infinity is rigorously satisfied. Making use of a scaling center the geometry of the problems is transformed into the scaled boundary coordinates including radial and circumferential coordinates. The boundary of the problem represents the computational domain. The finite-element approximation on the circumferential coordinates leads to the analytical equation in the radial coordinate.It is the goal of this paper to employ the method for soil-structure interaction analysis under seismic loads. The formulation of the method for seismic loadings is detailed for both bounded and unbounded problems. The structure is coupled with the unbounded domain on soil-structure interface. To demonstrate the applicability, simplicity and accuracy of the method, numerical examples modelled with the scaled boundary finite-element method are addressed. The results are compared with the results obtained from the commercial finite-element software SAP. Good agreement is achieved.

Keywords:
Dynamic soil-structure interaction;
Scaled boundary finite-element method;
Unbounded domains;
Seismic loads

1. Introduction

A structure interacts with the supporting soil under dynamic actions, such as impacts and earthquakes. Dynamic soil-structure interaction analysis plays an important role in the design and safety assessment of structures, especially for large-scale spatial structures, such as dams, nuclear power plants, high-rise buildings and bridges. In a soil-structure system, the volume of soil is much larger than the structure's, so the soil-structure interaction should be considered. This system of the structure and soil can be subjected to static or dynamic loads. In statics, the unbounded domain can be truncated sufficiently far away from the structure, as the stress and displacement amplitudes decrease with increasing the distance from the structure. However, in dynamics it is not the case, and this procedure cannot be applied. The truncated boundary reflects the waves coming from the source of vibrations while they must propagate toward infinity. This reflection affects the actual response of the structure. To analyze the system of soil-structure interaction, the infinite soil is divided into an irregular bounded soil that can exhibit nonlinear behaviour and a regular unbounded soil that extends to infinity and behaves linearly. The bounded domain including the structure and the irregular bounded soil can be modelled by the well-developed finite-element method. The most challenging part of a soil-structure interaction analysis is modelling the regular unbounded soil. There is an important consequence in wave

dynamics: waves which are moving toward infinity are not reflected back to the domain. Boundary conditions should be enforced on the boundary to absorb the incoming waves [1].

There are two main methods for dynamic analysis of soil-structure interaction problems. Direct method is the easiest way to analyze this interaction. In this method, local boundary conditions are used. It leads to an approximate method. To capture the infinity with a sufficient accuracy, the unbounded domain is truncated sufficiently far away from the structure and approximate boundary conditions are enforced on it [1-2]. Substructure method is an accurate method comparing with the direct method so the computational domain can be smaller than that for the direct method. As the artificial boundary conditions are so close to the structure, more exact boundary conditions have to be enforced on the boundary. When the boundary condition is exact, it can be applied directly on the soil-structure interface. In this method, normally, the exact boundary conditions are expressed as dynamic-stiffness matrix $[S^{\infty}(\omega)]$ on the boundary in the frequency domain. In the time domain, displacement unit impulse including convolution integrals represents the exact boundary conditions $[S^{\infty}(t)]$.

Various methods have been proposed in the literature for the solution of wave equations in unbounded domains. In general, these approaches are classified into two broad categories: global and local procedures [1-2]. Global procedures are divided into the boundary element method [3], thin layer method [4], exact non-reflecting boundary conditions [5-6] and the scaled boundary finite-element method [7]. Local procedures are divided into transmitting boundary conditions [8-9], infinite elements [10-11] and absorbing layers [12]. Global procedures are used in the substructure method and local procedures are used in the direct method.

The scaled boundary finite-element method has been originally developed for the dynamic analysis of unbounded domains. It was named at that time the consistent infinitesimal finite-element cell method as the original derivation for two-dimensional scalar waves was mechanical-based. A finite-element cell with the exterior boundary similar to the interior one was introduced in the radial direction adjacent to the structure-medium interface. The relationship based on similarity and the limit of the infinitesimal cell width tending to zero led to the consistent infinitesimal finite-element cell equation. This equation was derived in the frequency domain and then transformed into the time domain. This technique was later extended to two-dimensional vector waves [13] and three-dimensional waves [14]. Wolf and Song [15] applied this technique to two and three-dimensional statics, dynamics and diffusion in unbounded and bounded media. The crack tip stress intensity factors in fracture mechanics were also calculated.

Starting from the governing partial differential equations and the scaled boundary transformation, a new derivation consistent with that of the conventional finite-element method (FEM) was developed. With the new derivation, the method was re-named Scaled Boundary Finite-Element Method (SBFEM) for the first time. The original derivation of the scaled boundary finite-element equations was based on Galerkin's weighted residual method. Deeks and Wolf [16] later used the principal of virtual work to re-derive the scaled boundary finite-element equations. The method was extended to model body loads in [17]. For certain distribution of body loads, the concentrated loads and loads varying as power function of radial coordinate, analytical solutions were derived. Deeks presented a procedure to enforce side-face displacements approximated by a power series in the scaled boundary finite-element method [18]. Bazyar and Song [19-20] extended the scaled boundary finite-element method to model time-harmonic and transient response of non-homogeneous elastic unbounded domains. They later developed new techniques to enhance the solution procedures for modelling unbounded domains in frequency and time domains [21-22]. In this paper, the scaled boundary finite-element method is employed to model soil-structure interaction problems under seismic loads.

The outline of the paper is as follows: Summary of the scaled boundary finite-element method is presented in Section 2. The coupling of the bounded and unbounded domains in time domain under seismic loading is addressed in Section 3. Numerical examples are presented in Section 4. Conclusions are stated in Section 5.

2. Summary of the Scaled Boundary Finite-Element Method

The scaled boundary finite-element formulation for elasto-dynamics in both frequency and time domains is detailed in [1]. Only a brief summary of the formulations and solution procedures in 2D problems is presented in this section.

In the scaled boundary finite-element method, a so-called scaling centre O is chosen in a zone from which the whole boundary is visible, see Figure (1a). Only the boundary S directly visible from the scaling centre is discretized (see Figure (1b), for typical line element to be used for two-dimensional problems and Figure (1c) for a typical surface element to be used for three-dimensional problems). The nodal coordinates of an element in the Cartesian coordinate system are arranged in $\{x\}$ and $\{y\}$. The geometry of the element is interpolated using the shape functions $[N(\eta)]$ formulated in the local coordinates η. The geometry of the domain is defined by scaling the boundary with the dimensionless radial coordinate ξ pointing from the scaling centre O to a point on the boundary, see Figure (1a). At the scaling centre and on the boundary, ξ is chosen equal to 0 and 1, respectively. Unbounded domains are defined with ξ between 1 on the interface and ∞ at the infinity. A point $(\hat{x}, \hat{y})$ inside the domain is expressed as (see Figure (1a)):

$$\hat{x}(\xi,\eta)\} = \xi[N(\eta)]\{x\} \tag{1a}$$

$$\hat{y}(\xi,\eta)\} = \xi[N(\eta)]\{y\} \tag{1b}$$

ξ, η are called the scaled boundary coordinates. The change of coordinates from $\hat{x}$, $\hat{y}$ to ξ, η is called the scaled boundary transformation.

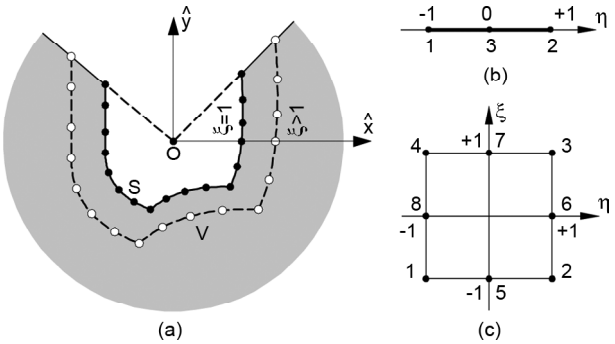

Figure 1. (a) Representation of an unbounded domain in the scaled boundary finite-element method; (b) three-node line element on boundary; and (c) eight-node surface element on boundary.

Along the radial lines passing through the scaling centre O and a node on the boundary, the nodal displacement functions $\{u(\xi)\}$ are introduced. The directions of the displacement components are defined in the original Cartesian coordinates as in the standard finite-element method. Isoperimetric displacement elements are used in the circumferential directions. The displacements at a point (ξ, η) are interpolated piece-wisely from the displacement functions $\{u(\xi)\}$

$$\begin{aligned}&\{u(\xi,\eta,\zeta)\} = [N^u(\eta,\zeta)]\{u(\xi)\} = \\ &[N_1(\eta,\zeta)[I], N_2(\eta,\zeta)[I],...]\{u(\xi)\}\end{aligned} \tag{2}$$

where $[I]$ is a 2×2 identity matrix. Once the governing differential equations were expressed in the scaled boundary coordinates, the Galerkin's weighted residual technique or the virtual work method is applied in the circumferential direction η. After assembling the element equations, the scaled boundary finite-element (SBFE) equation in displacement is formulated in the frequency domain for two- and three-dimensional problems as

$$\begin{aligned}&[E^0]\xi^2\{u(\xi)\}_{,\xi\xi} + \\ &((s-1)[E^0]-[E^1]+[E^1]^T)\,\xi\{u(\xi)\}_{,\xi} + \\ &((s-2)[E^1]^T-[E^2])\{u(\xi)\} + \\ &(\omega\xi)^2[M^0]\{u(\xi)\} = 0\end{aligned} \tag{3}$$

where s(=2 or 3) denotes the spatial dimension of the domain. $[E^0],[E^1],[E^2]$ and $[M^0]$ are coefficient matrices obtained by assembling the element coefficient matrices as in the finite-element method

$$[E^0] = \int_{-1}^{+1}[B^1(\eta)]^T[D(\eta)][B^1(\eta)]|J(\eta)|d\eta \tag{4a}$$

$$[E^1] = \int_{-1}^{+1}[B^2(\eta)]^T[D(\eta)][B^1(\eta)]|J(\eta)|d\eta \tag{4b}$$

$$[E^2] = \int_{-1}^{+1}[B^2(\eta)]^T[D(\eta)][B^2(\eta)]|J(\eta)|d\eta \tag{4c}$$

$$[M^0] = \int_{-1}^{+1}[N(\eta)]^T\rho[N(\eta)]|J(\eta)|d\eta \tag{4d}$$

in which $[B^1(\eta)]$ and $[B^2(\eta)]$ are the nodal displacement-strain relationship matrices. Integrations are performed over the elements on boundary (at $\xi=1$) only. $[E^0]$ and $[M^0]$ are positive-definite and

symmetric and $[E^2]$ is symmetric. The amplitude of nodal forces $\{R(\xi)\}$ on a surface is calculated as in the finite-element method by integrating the surface tractions over the circumferential directions η.

$$\{R(\xi)\} = -\xi^{s-1}\left([E^0]\{u(\xi)\}_{,\xi} + \frac{1}{\xi}[E^1]^T\{u(\xi)\}\right) \quad (5)$$

The dynamic-stiffness matrix $[S^\infty(\omega)]$ relates the amplitudes of the nodal forces $\{R(\xi)\}$ to those of the displacements $\{u(\xi)\}$ ($\{R(\xi)\} = [S^\infty(\omega)]\{u(\xi)\}$). Eliminating $\{R(\xi)\}$ and $\{u(\xi)\}$ from equations, (3) and (5) leads to an equation for the dynamic-stiffness matrix $[S^\infty(\omega)]$ on the boundary ξ =1.

$$\begin{aligned}&([S^\infty(\omega)]+[E^1])[E^0]^{-1}([S^\infty(\omega)]+[E^1]^T)-\\&(s-2)[S^\infty(\omega)]-\omega[S^\infty(\omega)]_{,\omega}-\\&[E^2]+\omega^2[M^0]=0\end{aligned} \quad (6)$$

Eq. (6) is a system of nonlinear first-order ordinary differential equations in the independent variable ω to be solved numerically for the dynamic-stiffness matrix.

2.1. Solution Procedure for a Frequency-Domain Analysis

The radiation condition at infinity is satisfied using an asymptotic expansion of the dynamic-stiffness matrix for high frequency as:

$$[S^\infty(\omega)] = [K_\infty] + i\omega[C_\infty] + \sum_{i=1}^{m}[A^{(i)}](i\omega)^{-i} \quad (7)$$

The first two terms on the right-hand side represent the singular term. The regular term is expanded as a power series of order m in $i\omega$. Coefficient matrices $[C_\infty], [K_\infty]$ and $[A^{(i)}]$ are determined by constructing a general Eigen-value problem ($\langle\bullet\rangle$ stands for a diagonal matrix) [10]:

$$[M^0][\Phi] = [E^0][\Phi]\langle\lambda^2\rangle \quad (8)$$

As the asymptotic power series solution, see Eq. (7), is only valid at high frequency, the dynamic-stiffness matrix at low and intermediate frequencies has to be evaluated by integrating Eq. (6) numerically. In an actual calculation, the dynamic-stiffness matrix at a specified high frequency ω_h, $[S^\infty(\omega_h)]$, is approximated by the asymptotic expansion in Eq. (7). $[S^\infty(\omega_h)]$ is then used as the starting value to integrate the scaled boundary finite-element equation in dynamic stiffness, Eq. (6), for decreasing ω to obtain the dynamic-stiffness matrix over the complete frequency range. To avoid this computationally expensive task of numerical integration, a Pade' series and a continued-fraction solution for the dynamic-stiffness matrix were developed in [21-22] directly from the SBFE equation.

2.2. Solution Procedure for a Time-Domain Analysis

The original derivation of the SBFE equation in time domain is detailed in [15]. Here, a brief summary is provided. The interaction force-acceleration relationship in the frequency domain is formulated as:

$$\{R(\omega)\} = [M^\infty(\omega)]\{\ddot{u}(\omega)\} = [M^\infty(\omega)](i\omega)^2\{u(\omega)\} \quad (9)$$

From Eq. (9) and the definition of dynamic-stiffness matrix ($\{R(\omega)\} = [S^\infty(\omega)]\{u(\omega)\}$) on the boundary, the relationship between the acceleration and the displacement dynamic-stiffness matrix is obtained as:

$$[S^\infty(\omega)] = (i\omega)^2[M^\infty(\omega)] \quad (10)$$

The interaction force-acceleration relationship is expressed in the time domain as:

$$\{R(t)\} = \int_0^t [M^\infty(t-\tau)]\{\ddot{u}(\tau)\}d\tau \quad (11)$$

where $[M^\infty(t)]$ is the acceleration unit-impulse response matrix. $[M^\infty(t)]$ and $[M^\infty(\omega)]$ form a Fourier transform pair. Substituting Eq. (10) in Eq. (6) and performing the inverse Fourier transformation of the resulting equation leads to the SBFE equation in time domain involving the convolution integrals as:

$$\begin{aligned}&\int_0^t [m^\infty(t-\tau)][m^\infty(\tau)]d\tau +\\&t\int_0^t [m^\infty(\tau)]d\tau + [e^1]\int_0^t\int_0^\tau [m^\infty(\tau')]d\tau' d\tau +\\&\int_0^t\int_0^\tau [m^\infty(\tau')]d\tau' d\tau [e^1]^T - \frac{t^3}{6}[e^2]H(t) -\\&t[m^0]H(t) = 0\end{aligned} \quad (12)$$

where

$$[m^\infty(t)] = ([U]^{-1})^T[M^\infty(t)][U]^{-1} \quad (13)$$

and $H(t)$ is the Heaviside-step function. The

upper-triangular matrix $[U]$ is determined from the decomposition of the coefficient matrix $[E^0]$ as:

$$[E^0]=[U]^T[U] \tag{14a}$$

$$[e^1]=([U]^{-1})^T[E^1][U]^{-1}-(\frac{s+1}{2})[I] \tag{14b}$$

$$[e^2]=([U]^{-1})^T([E^2]-[E^1][E^0]^{-1}[E^1]^T)[U]^{-1} \tag{14c}$$

$$[m^0]=([U]^{-1})^T[M^0][U]^{-1} \tag{14d}$$

The time-discretization method is used to solve Eq. (12) for $[m^\infty(t)]$ [15]. The acceleration unit-impulse response matrix $[M^\infty(t)]$ is then determined as:

$$[M^\infty(t)]=[U]^T[m^\infty(t)][U] \tag{15}$$

To circumvent the convolution integral in a time-domain analysis of unbounded domains, the continued-fraction solution of the dynamic-stiffness matrix was developed in [22].

The equation of motion of both bounded and unbounded domains are formulated as that in classical structural dynamics, i.e. a system of ordinary differential equations with time-independent coefficient matrices. This new solution procedure permits the application of standard time-stepping schemes to perform a transient analysis.

In the sub-structure method for dynamic analysis of problems involving soil-structure interactions, the nodal force-displacement relationships for the bounded domain and the unbounded domain are derived separately and coupled at the soil-structure interface. Section 3 deals with the coupling of bounded and unbounded domains under seismic loadings in the time domain.

3. Coupling of Bounded and Unbounded Domains under Seismic Loads in Time Domain

In the substructure method as shown in Figure (2), the nodal force-displacement relationships for the bounded domain and the unbounded domain are derived separately and coupled at the generalized structure-soil interface. The equation of motion of the bounded domain can be written as:

$$\begin{bmatrix}[M_{ss}] & [M_{sb}]\\ [M_{bs}] & [M_{bb}]\end{bmatrix}\begin{Bmatrix}\{\ddot{u}_s(t)\}\\ \{\ddot{u}_b(t)\}\end{Bmatrix}+\begin{bmatrix}[C_{ss}] & [C_{sb}]\\ [C_{bs}] & [C_{bb}]\end{bmatrix}\begin{Bmatrix}\{\dot{u}_s(t)\}\\ \{\dot{u}_b(t)\}\end{Bmatrix}+\begin{bmatrix}[K_{ss}] & [K_{sb}]\\ [K_{bs}] & [K_{bb}]\end{bmatrix}\begin{Bmatrix}\{u_s(t)\}\\ \{u_b(t)\}\end{Bmatrix}=\begin{bmatrix}\{P_s(t)\}\\ \{P_b(t)\}-\{R_b(t)\}\end{bmatrix} \tag{16}$$

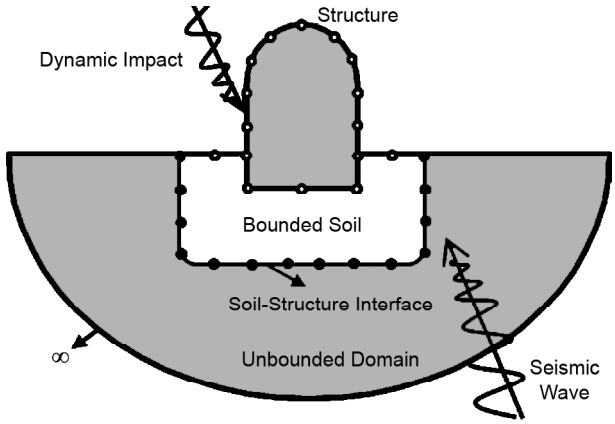

Figure 2. Soil-structure interaction analysis by sub-structure method.

where $[M]$, $[C]$ and $[K]$ are mass, material damping and static-stiffness matrices of bounded domains, respectively; $\{u(t)\}, \{\dot{u}(t)\}$ and $\{\ddot{u}(t)\}$ are displacement, velocity and acceleration vectors, respectively. $\{P(t)\}$ is the external load vector. The subscripts s and b denote the nodes of the bounded domain and nodes associated with the generalized structure-soil interface, respectively, see Figure (2). $\{R_b(t)\}$ is the interaction force vector which represents the contribution of the unbounded domain on the structure-soil interface and is expressed as:

$$\{R(t)\}=\int_0^t[M^\infty(t-\tau)]\{\ddot{u}(\tau)\}d\tau \tag{17}$$

where $[M^\infty(t)]$ to be determined from Eqs. (12) and (15).

In this paper, the bounded domain is also modelled using the scaled boundary finite-element method. The same equation as Eq. (6) is derived for bounded domains with only sign differences as:

$$\begin{aligned}&([S^b(\omega)]-[E^1])[E^0]^{-1}([S^b(\omega)]-\\ &[E^1]^T)+(s-2)[S^b(\omega)]+\\ &\omega[S^b(\omega)]_{,\omega}-[E^2]+\omega^2[M^0]=0\end{aligned} \tag{18}$$

Static-stiffness matrix $[K]=[S^b(\omega=0)]$ in Eq. (16), is obtained from an Eigen-value problem resulted from Eq. (18) for $\omega=0$ as detailed in [15]. The mass matrix $[M]$ is determined by assuming low frequency behaviour for bounded domains as:

$$[S^b(\omega)]=[K]-\omega^2[M] \tag{19}$$

Substituting Eq. (19) into Eq. (18) leads to a Lyapunov equation to be solved for mass matrix

(Reference [15] is advised for the details). Material damping $[C]$ can be determined using the Rayleigh method as in the finite-element method.

To take into account the seismic forces, in Eq. (17), dynamic force is applied as seismic acceleration $\{\ddot{u}_b^g(t)\}$ leading to interaction force vector on the soil-structure interface as:

$$\{R_b(t)\} = \int_0^t [M_b^\infty(t-\tau)]\{\ddot{u}_b(\tau) - \ddot{u}_b^g(\tau)\}d\tau \tag{20}$$

Having substituted Eq. (20) into Eq. (16), the time integration can be performed by the Newmark method with the parameters γ and β. The predictors for displacements and velocities are expressed as:

$$\begin{Bmatrix}\{u_s\}_n\\ \{u_b\}_n\end{Bmatrix} = \begin{Bmatrix}\{\hat{u}_s\}_n\\ \{\hat{u}_b\}_n\end{Bmatrix} + \beta\Delta t^2\begin{Bmatrix}\{\ddot{u}_s\}_n\\ \{\ddot{u}_b\}_n\end{Bmatrix} \tag{21a}$$

$$\begin{Bmatrix}\{\dot{u}_s\}_n\\ \{\dot{u}_b\}_n\end{Bmatrix} = \begin{Bmatrix}\{\hat{\dot{u}}_s\}_n\\ \{\hat{\dot{u}}_b\}_n\end{Bmatrix} + \gamma\Delta t\begin{Bmatrix}\{\ddot{u}_s\}_n\\ \{\ddot{u}_b\}_n\end{Bmatrix} \tag{21b}$$

$$\begin{Bmatrix}\{\hat{u}_s\}_n\\ \{\hat{u}_b\}_n\end{Bmatrix} = \begin{Bmatrix}\{u_s\}_{n-1}\\ \{u_b\}_{n-1}\end{Bmatrix} + \Delta t\begin{Bmatrix}\{\dot{u}_s\}_{n-1}\\ \{\dot{u}_b\}_{n-1}\end{Bmatrix} + (0.5-\beta)\Delta t^2\begin{Bmatrix}\{\ddot{u}_s\}_{n-1}\\ \{\ddot{u}_b\}_{n-1}\end{Bmatrix} \tag{22a}$$

$$\begin{Bmatrix}\{\hat{\dot{u}}_s\}_n\\ \{\hat{\dot{u}}_b\}_n\end{Bmatrix} = \begin{Bmatrix}\{\dot{u}_s\}_{n-1}\\ \{\dot{u}_b\}_{n-1}\end{Bmatrix} + (1-\Delta t)\begin{Bmatrix}\{\ddot{u}_s\}_{n-1}\\ \{\ddot{u}_b\}_{n-1}\end{Bmatrix} \tag{22b}$$

where Δt is the time step. Eq. (20) is discretized with respect to time as:

$$\begin{aligned}&\{R_b\}_n = \\ &\sum_{j=1}^{n}[M_b^\infty]_{n-j+1}\int_{t_{j-1}}^{t_j}\{\ddot{u}_b(\tau) - \ddot{u}_b^g(\tau)\}d\tau = \\ &\sum_{j=1}^{n}[M_b^\infty]_{n-j+1}\left(\int_{t_{j-1}}^{t_j}\{\ddot{u}_b(\tau)\} - \int_{t_{j-1}}^{t_j}\{\ddot{u}_b^g(\tau)\}\right)d\tau = \\ &\sum_{j=1}^{n}[M_b^\infty]_{n-j+1}\left(\{\dot{u}_b\}_n - \{\dot{u}_b\}_{n-1} - \frac{\{\ddot{u}_b^g\}_n - \{\ddot{u}_b^g\}_{n-1}}{2}\Delta t\right)\end{aligned} \tag{23}$$

Integral of $\{\ddot{u}_b^g(t)\}$ is obtained by an average manner. Substituting Eqs. (21b) and (22b) into the n^{th} term in the above series the interaction forces are reformulated as:

$$\{R_b\}_n = \gamma\Delta t[M_b^\infty]_1\{\ddot{u}_b\}_n + \{F_b\}_n \tag{24}$$

$$\begin{aligned}\{F_b\}_n = &(1-\gamma)\Delta t[M_b^\infty]_1\{\ddot{u}_b\}_{n-1} - \\ &[M_b^\infty]_1\frac{\{\ddot{u}_b^g\}_n + \{\ddot{u}_b^g\}_{n-1}}{2}\Delta t + \sum_{j=1}^{n-1}[M_b^\infty]_{n-j+1}\times \\ &\left(\{\dot{u}_b\}_j - \{\ddot{u}_b\}_{j-1} - \frac{\{\ddot{u}_b^g\}_j + \{\ddot{u}_b^g\}_{j-1}}{2}\Delta t\right)\end{aligned} \tag{25}$$

where $\{F_b\}_n$ depends on the response at previous time steps and is known at time station *n*.

Substituting Eqs. (21) and (24) into Eq. (16) results in:

$$\begin{aligned}&\begin{bmatrix}[D_{ss}] & [D_{sb}]\\ [D_{bs}] & [D_{bb}] + \gamma\Delta t[M_b^\infty]_1\end{bmatrix}\begin{Bmatrix}\{\ddot{u}_b\}_n\\ \{\ddot{u}_s\}_n\end{Bmatrix} = \\ &\begin{Bmatrix}\{P_s\}_n\\ \{P_b\}_n - \{F_b\}_n\end{Bmatrix} - \begin{bmatrix}[K_{ss}] & [K_{sb}]\\ [K_{bs}] & [K_{bb}]\end{bmatrix}\begin{Bmatrix}\{\hat{u}_s\}_n\\ \{\hat{u}_s\}_n\end{Bmatrix} - \\ &\begin{bmatrix}[C_{ss}] & [C_{sb}]\\ [C_{bs}] & [C_{bb}]\end{bmatrix}\begin{Bmatrix}\{\hat{\dot{u}}_b\}_n\\ \{\hat{\dot{u}}_s\}_n\end{Bmatrix}\end{aligned} \tag{26}$$

where the effective stiffness $[D]$ of the coupled system is expressed as:

$$\begin{aligned}&\begin{bmatrix}[D_{ss}] & [D_{sb}]\\ [D_{bs}] & [D_{bb}]\end{bmatrix} = \begin{bmatrix}[M_{ss}] & [M_{sb}]\\ [M_{bs}] & [M_{bb}]\end{bmatrix} - \\ &\gamma\Delta t\begin{bmatrix}[C_{ss}] & [C_{sb}]\\ [C_{bs}] & [C_{bb}]\end{bmatrix} - \beta\Delta t^2\begin{bmatrix}[K_{ss}] & [K_{sb}]\\ [K_{bs}] & [K_{bb}]\end{bmatrix}\end{aligned} \tag{27}$$

At time station n, the terms at the right-hand side of Eq. (26) are known. Having obtained the accelerations from Eq. (26), the displacements and velocities can be determined from Eqs. (21). Note that in the above equations $\{u(t)\}, \{\dot{u}(t)\}$ and $\{\ddot{u}(t)\}$ are absolute displacement, velocity and acceleration vectors, respectively.

In the case of rigid foundations, no soil is considered under the structure, and the structure is assumed as a bounded domain. No interaction between the structure and the soil is available. Equation of motion of bounded domains in time domain is expressed as:

$$[M]\{\ddot{u}_s(t)\} + [C]\{\dot{u}_s(t)\} + [K]\{u_s(t)\} = \{P(t)\} \tag{28}$$

In the absence of dynamic external forces, dynamic force is applied as seismic acceleration $\{\ddot{u}_g(t)\}$ leading to:

$$\begin{aligned}&[M]\{\ddot{u}_s(t)\} + [C]\{\dot{u}_s(t)\} + [K]\{u_s(t)\} = \\ &-[M]\{\ddot{u}_g(t)\}\end{aligned} \tag{29}$$

The time integration can be performed by the well-known Newmark method.

4. Numerical Examples

To illustrate the effect of soil-structure interaction on dynamic response of structures and to demonstrate the simplicity and accuracy of the scaled boundary finite-element method (SBFEM), two examples are addressed. For each example, two cases are taken into consideration:

a) Rigid foundation: in this case, the soil is neglected and the base is assumed to be fixed. The results are verified by the finite-element method (FEM) using the commercial software SAP 2000 [23].
b) Flexible foundation: in this case, the unbounded soil is considered and the effect of interaction between the soil and the structure is investigated. The results are compared with the results obtained from SAP 2000 and the ability of the scaled boundary finite-element method in modelling unbounded domains is illustrated.

Acceleration time history of Tabas earthquake shown in Figure (3) is considered as seismic input motion in both examples.

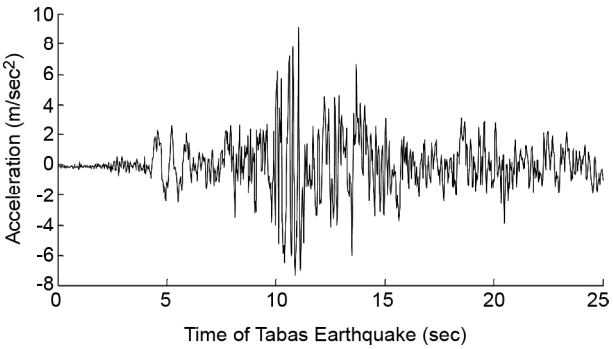

Figure 3. Acceleration time history of Tabas earthquake.

4.1. A Frame-Like Structure

For the first example, a frame-like structure shown in Figure (4) is analyzed. This example is designed to introduce the concept of soil-structure interaction and to illustrate the effect of soil-structure interaction on the dynamic response of structures. For simplicity, the dimensions of the structure and material properties of both the structure and the foundation to be detailed later are selected in a dimensionless fashion. A consistent set of units is used in the analysis. Plane stress condition is considered. The material properties are defined by the

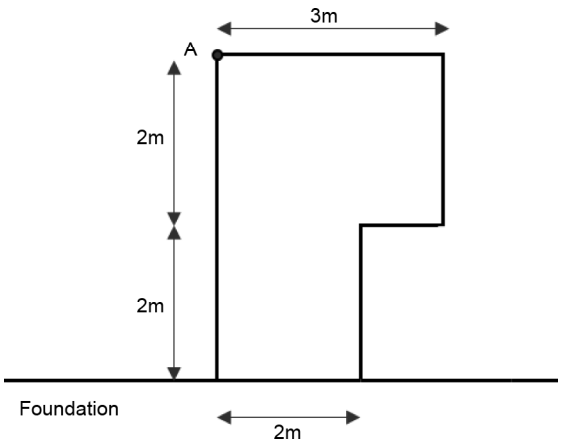

Figure 4. Geometry of a frame-like structure.

modulus of elasticity $E=10^4$, Poisson's ratio $v=0.2$ and mass density $\rho=1$. The analyses are performed directly in the time domain by using the time integration Newmark method with $\gamma=0.25$ and $\beta=0.5$.

Both rigid and flexible foundations are considered. In the case of the rigid foundation, the base of the structure is assumed to be fixed. In the scaled boundary finite-element analysis, one sub-domain is introduced, see Figure (5a). The scaling centre is chosen at the inner corner $C1$. The boundaries of the sub-domain are discretized with three-node elements. Side faces passing through the scaling centre are not discretized. Acceleration time history of Tabas earthquake is applied. The time step is selected as $\Delta t=0.01$. An extended finite-element analysis is also performed using commercial software SAP 2000 to provide a reference solution. The mesh consisting of four-node rectangular elements is shown in Figure (5b). The density of the finite-element mesh on the boundary is the same as the scaled boundary finite-element mesh.

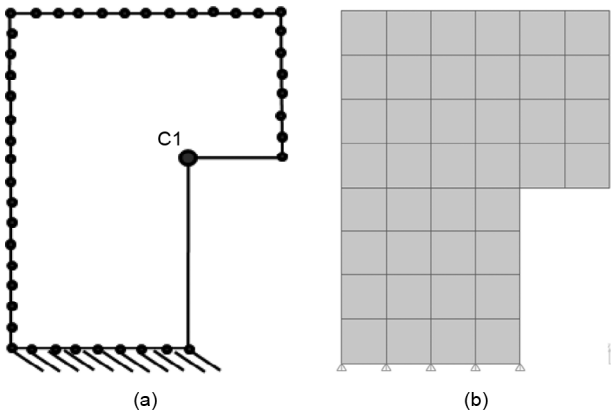

Figure 5. Mesh for the frame-like structure on rigid foundation: (a) SBFE mesh; (b) FE mesh.

The horizontal displacement at point A on left top of the structure shown in Figure (4) is plotted in Figure (6). As there is no material damping for the structure and the rigid foundation is assumed, it is observed that the response of the structure is not damped. The results obtained from SBFEM and FEM agree very well, showing the ability of the scaled boundary finite-element method for modelling bounded domain problems.

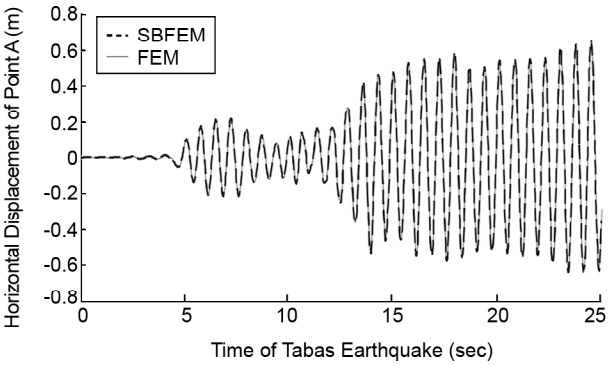

Figure 6. Horizontal displacement at point A of the frame-like structure.

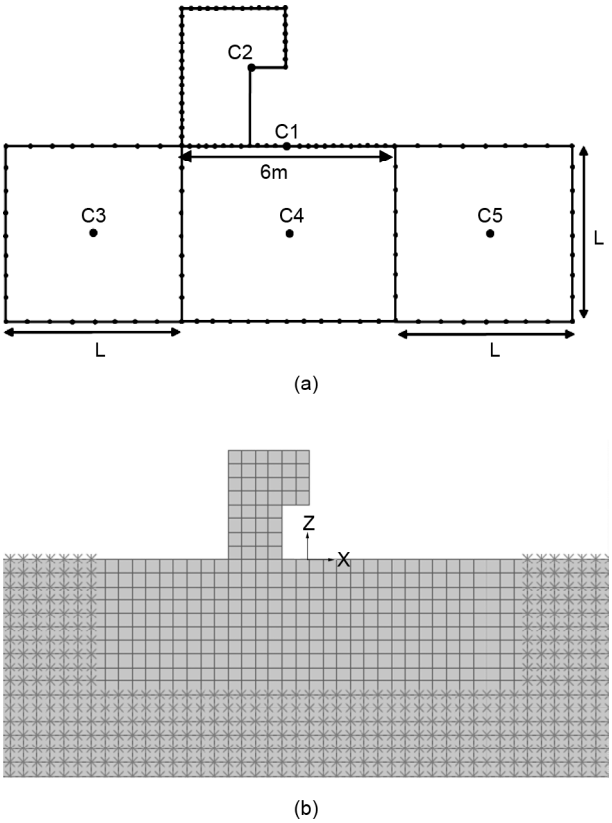

Figure 7. Mesh for the frame-like structure on flexible foundation: (a) SBFE mesh; (b) FE mesh.

In the case of the flexible foundation, it is assumed that the structure is resting on a half-plane, and the material properties are defined by the modulus of elasticity $E = 2400$, Poisson's ratio $v = 0.2$ and the mass density $\rho = 1$. The scaled boundary finite-element mesh is shown in Figure (7). To satisfy similarity condition, a part of the unbounded domain surrounding the structure is modelled as bounded domains. Here, three bounded sub-domains are introduced. The scaling centres are located at the centres of the sub-domains (C3, C4 and C5). The remaining part of the half-plane is modelled as an unbounded domain. Its scaling center is chosen at C1. A scaled boundary finite-element analysis with the mesh with length $L = 5$, see Figure (7a), is performed. An extended finite-element analysis is performed using SAP 2000 to provide a reference solution. The mesh consists of four-node rectangular elements is shown in Figure (7b). Simple Dirichlet boundary conditions are enforced on the truncated boundary far away from the soil-structure interface. The time step is selected as $\Delta t = 0.02$.

The horizontal displacement caused by seismic load at point A is portrayed in Figure (8). In the results obtained from the finite-element analysis, the

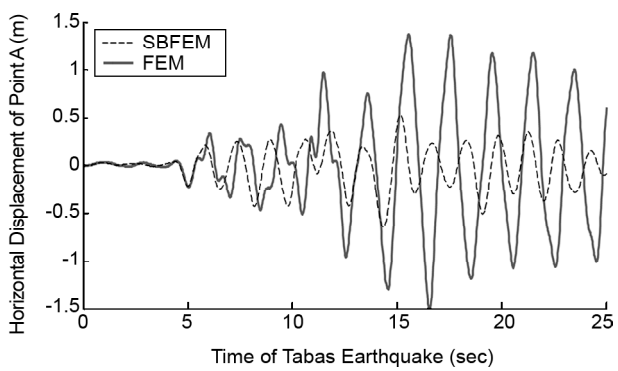

Figure 8. Horizontal displacement at point A of the frame-like structure on flexible foundation.

displacement is not damped, and the oscillation is occurred, see Figure (8). When the propagating waves impinge on the truncated boundary, they are reflected back toward inside the domain, and therefore, they disturb the response of the structure. However, in the scaled boundary finite-element method, propagating waves go to the infinity and will be absorbed there. The results obtained from the SBFEM and FEM are in an acceptable agreement by about 6s. After time $t = 6$, the waves reflected back from the truncated boundary in the finite-

element method contaminate the response of the structure.

It is observed by comparing Figure (6) with Figure (8) that the dynamic interaction between the structure and the foundation strongly affects the structure response. When the dynamic soil-structure interaction is considered for this example, the response is damped. The radiation damping of the unbounded domain leads to rapid decay of the vibration, see Figure (8). This phenomenon does not occur when the foundation is rigid, see Figure (6).

4.2. A DAM Located on a Half-Plane

For the second example, a real large-scale dam (Koyna Dam in China) located on a half-plane is examined. Real dimensions and material properties for the dam and the foundation are considered in this example. The geometry of the dam is shown in Figure (9).

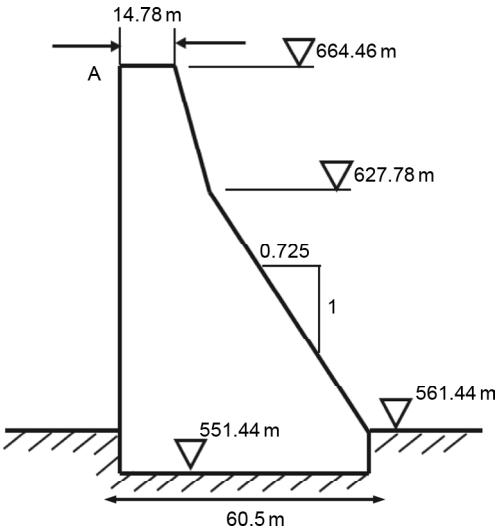

Figure 9. Geometry of the dam.

Plane-strain condition is considered. The analyses are performed directly in the time domain by using the Newmark method with $\beta = 0.25$ and $\gamma = 0.5$. Material properties are defined by the modulus of elasticity $E = 40$GPa, Poisson's ratio $v = 0.2$ and the mass density $\rho = 2600$ kg/m^3. Again, both rigid and flexible foundations are addressed. In the rigid case and in the scaled boundary finite-element analysis, the dam is divided into three sub-domains shown in Figure (10a). The scaling centers are C1, C2 and C3. Linear elements have used for mesh discritization resulting in 1296 degrees of freedom. Once more, the acceleration time history of Tabas earthquake is applied. The time step is selected as $\Delta t = 0.002$ s. A finite-element analysis is performed using the commercial finite-element software SAP 2000 to verify the validity of the SBFE results. The mesh used in the analysis has 32096 degrees of freedom. The density of the finite-element mesh is shown in Figure (10b).

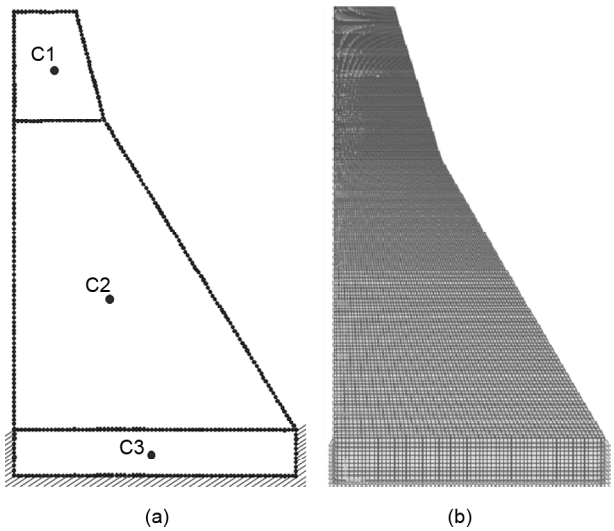

Figure 10. Dam on a rigid foundation: (a) Scaled boundary finite-element mesh ; (b) Finite-element mesh.

The horizontal displacement at point A is plotted in Figure (11). The scaled boundary finite-element results are in a reasonable agreement with the finite-element results obtained from SAP 2000. As it is observed again in this example, when the foundation is rigid, the response of the dam is not damped.

In the case of flexible foundation, it is assumed that the structure is resting on a half-plane with the

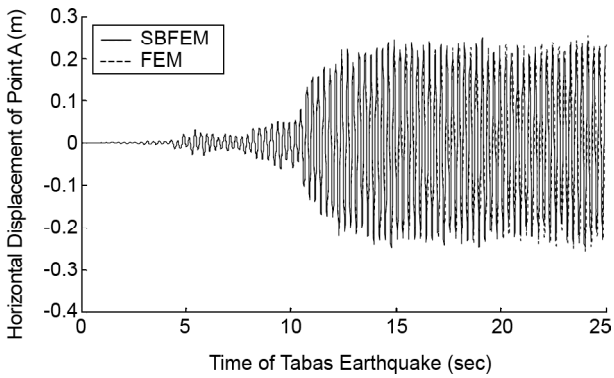

Figure 11. Horizontal displacement at point A of a dam on a rigid foundation.

modulus of elasticity $E = 30$ GPa, Poisson's ratio $v = 0.2$ and the mass density $\rho = 1900$ kg/m^3. The scaled boundary finite-element mesh is shown in Figure (12a). Yet again in this case, the dam is modeled as three bounded sub-domains. The scaling centres are located at the centres of the sub-domains (C2, C3 and C4). The half-plane is modeled as an unbounded domain. Its scaling centre is chosen at C1. Bounded domains (structure) and the unbounded domain are coupled at the interface between the structure and the half plane.

The horizontal displacement response at point A is plotted in Figure (13). To validate the accuracy of the SBFE results, an extended finite-element mesh is analyzed using SAP 2000. For more contrast, a close-up of the frame has been presented, see Figure (12b); however, for accurate results in a long time, the soil has to be extended to a much more depth. The results of the finite-element analysis are also portrayed in Figure (13). It is observed that two results agree well before the waves reflected at the outer boundary of the extended mesh reach the structure.

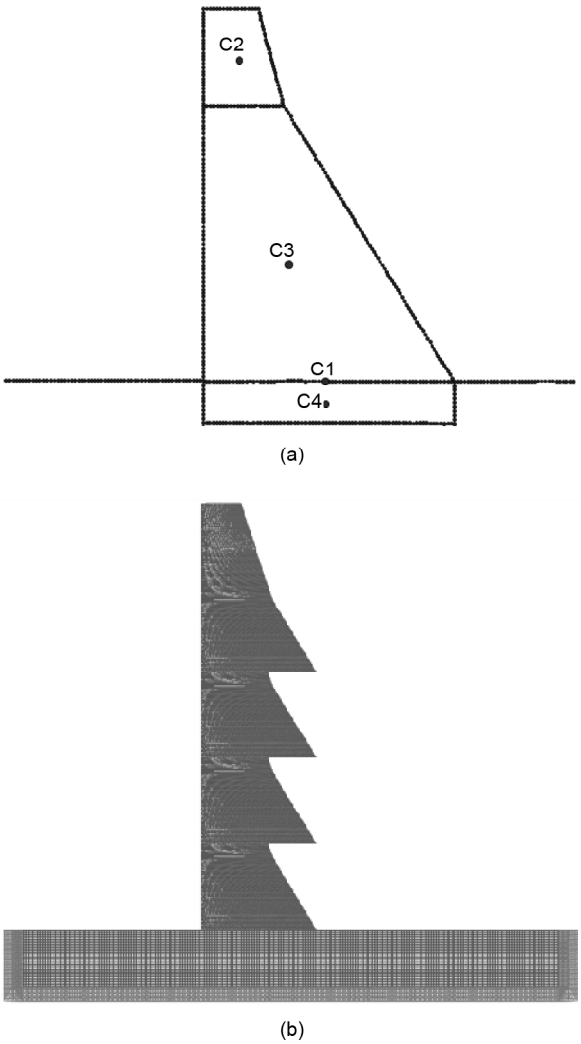

Figure 12. Dam on a flexible foundation: (a) Scaled boundary finite-element mesh; (b) Finite-element mesh (Sap).

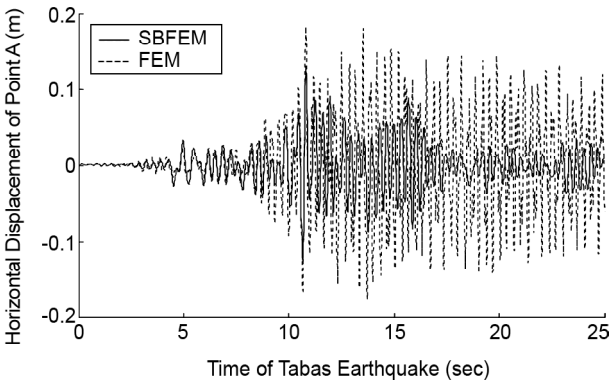

Figure 13. Horizontal displacement at point A of dam on flexible foundation.

By comparing Figures (11) and (13), the strong effect of dynamic interaction between the structure and the foundation on the response of the dam is observed. The radiation damping of the unbounded domain leads to rapid decay of the vibration as shown in Figure (13), while this phenomenon does not occur when the foundation is rigid as illustrated in Figure (11). No significant change in the amplitude of the displacement response is observed.

5. Conclusions

The scaled boundary finite-element method is employed to perform a dynamic soil-structure interaction analysis directly in the time domain. Seismic loads are applied to the structure as dynamic loads. Both bounded and unbounded domains are modelled with scaled boundary finite-element method. Only the boundary is discretized reducing the spatial dimension by one. Radiation condition at infinity is satisfied rigorously. No fundamental solution is needed. As only the boundary of the sub-domains is discretized, the mesh generation is simpler than the one in the finite element method. This also reduces the size of the equation of motion of the global system. Newmark implicit time integration method is used to perform the time integration. Finite-element analyses using commercial software SAP 2000 are carried out to verify the results of the scaled boundary finite-element method. Strong effect of soil-structure interaction on dynamic response of the structure is demonstrated. Numerical examples are

addressed to illustrate the accuracy and applicability of the scaled boundary finite-element method. Reasonable agreement with the results of the scaled boundary finite-element and the extended finite-element method is observed.

References

1. Bazyar, M.H. (2007). Dynamic Soil-Structure Interaction Analysis Using the Scaled Boundary Finite-Element Method, Ph.D Thesis, The Univ. of New South Wales, Sydney, Australia.
2. Wolf, J.P. (1985). Dynamic Soil-Structure Interaction, Prentice-Hall, Englewood Cliffs.
3. Brebbia, C.A., Telles, J.C.F., and Wrobel, L.C. (1984). Boundary Element Techniques, Springer-Verlag.
4. Lysmer, J. and Waas, G. (1972). Shear Waves in Plane Infinite Structures, *Journal of Engineering Mechanics*, **98**, 85-105.
5. Keller, J.B. and Givoli, D. (1989). Exact Non-Reflecting Boundary Conditions, *Journal of Computational Physics*, **82**, 172-192.
6. Tsynkov, S.V. (1998). Numerical Solution of Problems on Unbounded Domains: A Review, *Applied Numerical Mathematics*, **27**, 465.532.
7. Song, C. and Wolf, J.P. (1997). The Scaled Boundary Finite-Element Method Alias Consistent Infinitesimal Finite-Element Cell Method for Elasto-Dynamics, *Computational Methods in Applied Mechanics and Engineering*, **147**, 329-355.
8. Lysmer, J. and Kuhlemeyer, R.L. (1969). Finite Dynamic Model for Infinite Media, *Journal of Engineering Mechanics, ASCE*, **95**, 859.877.
9. Smith, W. D. (1974). A Nonreflecting Plane Boundary for Wave Propagation Problems, *Journal of Computational Physics*, **15**, 492-503.
10. Bettess, P. (1992). Infinite Elements, Penshaw Press, Sunderland, UK.
11. Astley, R. J. (2000). Infinite Elements for Wave Problems: A Review of Current Formulations and an Assessment of Accuracy, *International Journal for Numerical Methods in Engineering*, **49**, 951-976.
12. Israeli, M. and Orszag, S. (1981). Approximation of Radiation Boundary Conditions, *Journal of Computational Physics*, **41**, 115-135.
13. Wolf, J.P. and Song, Ch. (1995). Consistent Infinitesimal Finite-Element Cell Method: In-Plane Motion, *Computational Methods in Applied Mechanics and Engineering*, **123**, 355-370.
14. Song, Ch. and Wolf, J.P. (1996). Consistent Infinitesimal Finite-Element Cell Method: Three Dimensional Vector Wave Equation, *International Journal for Numerical Methods in Engineering*, **39**, 2189-2208.
15. Wolf, J.P. and Song, Ch. (1996). Finite-Element Modelling of Unbounded Media, John Wiley & Sons, Chichester.
16. Deeks, A.J. and Wolf, J.P. (2002). A Virtual Work Derivation of the Scaled Boundary Finite-Element Method for Elasto-Statics, *Computational Mechanics*, **28**, 489-504.
17. Song, C. and Wolf, J. P. (1999). Body Loads in the Scaled Boundary Finite-Element Method, *Computational Methods in Applied Mechanics and Engineering*, **180**, 117-135.
18. Deeks, A.J. (2004). Prescribed Side-Face Displacements in the Scaled Boundary Finite Element Method, *Computers and Structures*, **82**, 1153-1165
19. Bazyar, M.H. and Song, C. (2006). Time-Harmonic Response of Non-Homogeneous Elastic Unbounded Domains Using the Scaled Boundary Finite-Element Method, *Earthquake Engineering and Structural Dynamics*, **35**, 357-383.
20. Bazyar, M.H. and Song, Ch. (2006). Transient Analysis of Wave Propagation in Non-Homogeneous Elastic Unbounded Domains by Using the Scaled Boundary Finite-Element Method, *Earthquake Engineering and Structural Dynamics*, **35**, 1787-1806.
21. Song, Ch. and Bazyar, M.H. (2007). A Boundary Condition in Pade' Series for Frequency-Domain Solution of Wave Propagation in Unbounded Domains, *International Journal*

for Numerical Methods in Engineering, **69**, 2330-2358.

22. Bazyar, M.H and Song, Ch. (2008). A Continued-Fraction-Based High-Order Transmitting Boundary for Wave Propagation in Unbounded Domains of Arbitrary Geometry, *International Journal for Numerical Methods in Engineering*, **74**, 209-237.

23. SAP2000 (2007). Computers and Structures, Inc.